

5. WHICH FORMALISM TO USE FOR MODELING
VOLTAGE-DEPENDENT CONDUCTANCES ?

Alain Destexhe¹ and John Huguenard²

(1) Department of Physiology,
Laval University School of Medicine,
Québec G1K 7P4, Canada

(2) Department of Neurology and Neurological Sciences,
Stanford University Medical Center,
Stanford CA 94305, USA

Abbreviated title: "Different formalisms to model membrane currents"

Manuscript length: 8 figures, 30 pages (including captions)

Corresponding author:

Dr. A. Destexhe
Department of Physiology
Laval University
Pavillon F. Vandry
Québec G1K 7P4, Canada
Tel: (418) 656 5711
Fax: (418) 656 7898
email: alain@fmed.ulaval.ca

Contents

5.1	INTRODUCTION	3
5.2	DIFFERENT FORMALISMS TO MODEL ION CHANNELS	4
5.2.1	<i>The Hodgkin-Huxley model</i>	4
5.2.2	<i>Thermodynamic models</i>	6
5.2.3	<i>Markov models</i>	10
5.3	MODELS TO GENERATE ACTION POTENTIALS	12
5.3.1	<i>Models of Na⁺ and K⁺ currents underlying action potentials</i>	12
5.3.2	<i>Na⁺ currents in voltage-clamp</i>	13
5.3.3	<i>Genesis of action potentials</i>	14
5.4	FITTING MODELS TO VOLTAGE-CLAMP DATA	15
5.4.1	<i>Voltage-clamp characterization of the T-current</i>	15
5.4.2	<i>Hodgkin-Huxley model of the T-current</i>	16
5.4.3	<i>Linear thermodynamic model of the T-current</i>	17
5.4.4	<i>Nonlinear thermodynamic model of the T-current</i>	18
5.4.5	<i>Markov model of the T-current</i>	19
5.4.6	<i>Comparison of the different models</i>	21
5.5	CONCLUSION	21

5.1 INTRODUCTION

The selective permeability of neuronal membranes to ions is at the basis of various processes central to neurophysiology, such as the maintenance of a membrane potential, the genesis of neuronal excitability and the action of neurotransmitters and modulators. The rules governing ionic permeabilities were explored by Hodgkin, Huxley, Katz and others several decades ago. It was demonstrated that the ionic permeability of the membrane can be highly dependent on the membrane potential. Hodgkin and Huxley [1] characterized these properties of voltage-dependence and provided a mathematical model which proved that these properties were sufficient to account for the genesis of action potentials. The model of Hodgkin and Huxley was based on simple assumptions, reproduced well the behavior of the currents and its parameters are easy to determine from experimental data. This explains why Hodgkin-Huxley models are still widely used today, almost fifty years later.

Hodgkin and Huxley postulated that the membrane currents result from the assembly of gating particles freely moving in the membrane. The molecular components responsible for ionic permeabilities have been later identified as being transmembrane protein complexes containing a pore permeable specifically to one or several ionic species (reviewed in ref. [2]). These ion channels can have their permeability modulated by various factors, such as voltage or the binding of a ligand. The sensitivity of some ion channels to voltage is a fundamental property that constitutes the core mechanism underlying the electrical excitability of membranes, and is still today an important matter of investigation (for a recent review, see ref. [3]). Several types of voltage-dependent ion channels have been identified and are responsible for a rich repertoire of electrical behavior essential for neuronal function [4].

The biophysical properties of ion channels have been characterized in depth following the development of single-channel recording techniques (reviewed in ref. [5]). Single-channel recordings have shown that ion channels display rapid transitions between conducting and non-conducting states. It is now known that conformational changes of the channel protein give rise to opening/closing of the channel. Conformational changes of ion channels can be described by state diagrams analogous to the conformational changes underlying the action of enzymes. Markov models are based on such transition diagrams and have been used for modeling various types of ionic currents based on single-channel recordings (see ref. [5]). This formalism is more accurate than Hodgkin-Huxley models, but its drawback is the greater difficulty to estimate its parameters from experimental data. On the other hand, Markov models can also be used to draw simplified representations of the current, which only capture the most salient properties of voltage-dependent or synaptic interactions, more adequate for representing currents when simulating networks involving thousands of cells [6].

Thus, there exists various formalisms of different complexity to model ionic currents. Which formalism to adopt for modeling a given current depends on the experimental data available and its

accuracy, as well as on the desired level of precision in the behavior of the model. We illustrate these aspects in this chapter, by considering different types of formalisms to model processes such as the action potential and voltage-clamp recordings of the T-type calcium current in thalamic neurons. For both cases, we show the similarities and differences between the different models, how well they account for experimental data and which is the “minimal” model required to reproduce electrophysiological behavior.

5.2 DIFFERENT FORMALISMS TO MODEL ION CHANNELS

5.2.1 The Hodgkin-Huxley model

The formalism of Hodgkin and Huxley was introduced in 1952 to model the ionic interactions underlying action potentials. In a remarkable series of experiments on the squid giant axon, they determined that ionic conductances can be activated or inactivated according to the membrane potential. They used the technique of voltage-clamp, introduced earlier by Cole, to record the ionic currents generated at different voltages. They identified the kinetics of two voltage-dependent currents, the fast sodium current, I_{Na} , and the delayed potassium rectifier, I_K , mediated by Na^+ and K^+ , respectively. A mathematical model was necessary to establish that these properties of voltage-dependence were sufficient to explain the genesis of action potentials. The model introduced by Hodgkin and Huxley [1] incorporated the results of their voltage-clamp experiments and successfully accounted for the main properties of action potentials.

The starting point of the Hodgkin-Huxley model is the membrane equation describing three ionic currents in an isopotential compartment:

$$C_m \frac{dV}{dt} = -g_L (V - E_L) - g_{Na}(V) (V - E_{Na}) - g_K(V) (V - E_K), \quad (1)$$

where C_m is the membrane capacitance, V is the membrane potential, g_L , g_{Na} and g_K are the membrane conductances for leak currents, Na^+ and K^+ currents respectively, E_L , E_{Na} and E_K are their respective reversal potentials, which are given by the Nernst relation. For example, for K^+ ions:

$$E_K = \frac{RT}{ZF} \ln \frac{[K]_o}{[K]_i} \quad (2)$$

where R is the gas constant, T is the absolute temperature in degrees Kelvin, Z is the valence of the ion ($Z=1$ for K^+ ions, $Z=-1$ for Cl^- ions, etc), F is the Faraday constant, $[K]_o$ and $[K]_i$ are the concentration of K^+ ions outside and inside of the membrane, respectively (see Chapter 3).

The next step is to specify how the conductances $g_{Na}(V)$ and $g_K(V)$ depend on the membrane potential. Hodgkin and Huxley hypothesized that ionic currents result from the assembly of several independent gating particles which must occupy a given position in the membrane to allow the flow

of Na^+ or K^+ ions. Each gating particle can be in either side of the membrane and bears a net electronic charge such that the membrane potential can switch its position from the inside to the outside or vice-versa. The transition from these two states is therefore voltage-dependent, according to the diagram:



where α and β are respectively the forward and backward rate constants for the transitions from the outside to the inside position in the membrane. If m is defined as the fraction of particles in the inside position, and $(1 - m)$ as the fraction outside, one obtains the first-order kinetic equation:

$$\frac{dm}{dt} = \alpha_m(V) (1 - m) - \beta_m(V) m . \quad (4)$$

If one assumes that particles must occupy the inside position to conduct ions, then the conductance must be proportional to some function of m . In the case of squid giant axon, Hodgkin and Huxley [1] found that the nonlinear behavior of the Na^+ and K^+ currents, their delayed activation and their sigmoidal rising phase was best fit by assuming that the conductance is proportional to the product of several of such variables [1]:

$$g_{Na} = \bar{g}_{Na} m^3 h \quad (5)$$

$$g_K = \bar{g}_K n^4 , \quad (6)$$

where \bar{g}_{Na} and \bar{g}_K are the maximal values of the conductances and m , h , n represent the fraction of three different types of gating particles in the inside of the membrane. This equation allowed to fit voltage-clamp data of the currents accurately, which can be interpreted as that the assembly of 3 gating particles of type m and one of type h is required for Na^+ ions to flow through the membrane, while the assembly of 4 gating particles of type n is necessary for the flow of K^+ ions. These particles operate independently of each other, leading to the $m^3 h$ and n^4 forms.

When it was later established that ionic currents are mediated by the opening and closing of ion channels, the gating particles were reinterpreted as *gates* inside the pore of the channel. Thus, the reinterpretation of Hodgkin and Huxley's hypothesis was that the pore of the channel is controlled by four gates, that these gates operate independently of each other, and that all four gates must be open in order the channel to conduct ions.

The rate constants $\alpha(V)$ and $\beta(V)$ of m and n are such that depolarization promotes opening the gate, a process which is called *activation*. On the other hand, the rate constants of h are such that depolarization promotes closing of the gate¹, which process is called *inactivation*. Thus, the

¹and therefore closing of the entire channel because all gates must be open for the channel to conduct ions

experiments of Hodgkin and Huxley [1] established that three identical activation gates (m^3) and a single inactivation gate (h) are sufficient to explain the Na^+ current's characteristics. The K^+ current does not have inactivation and can be well described by four identical activation gates (n^4).

Taking together all the steps above, one can write the following set of equations [1]:

$$\begin{aligned} C_m \frac{dV}{dt} &= -g_L (V - E_L) - \bar{g}_{Na} m^3 h (V - E_{Na}) - \bar{g}_K n^4 (V - E_K) \\ \frac{dm}{dt} &= \alpha_m(V) (1 - m) - \beta_m(V) m \\ \frac{dh}{dt} &= \alpha_h(V) (1 - h) - \beta_h(V) h \\ \frac{dn}{dt} &= \alpha_n(V) (1 - n) - \beta_n(V) n , \end{aligned} \quad (7)$$

The rate constants (α_i and β_i) were estimated by fitting empirical functions of voltage to the experimental data [1]. These functions are given in Table 1.

Note that the Hodgkin-Huxley model is often written in a form more convenient to fit to experimental data. Eq. 4 can be rewritten in the form:

$$\frac{dm}{dt} = \frac{1}{\tau_m(V)} (m_\infty(V) - m) , \quad (8)$$

where

$$m_\infty(V) = \alpha(V) / [\alpha(V) + \beta(V)] \quad (9)$$

$$\tau_m(V) = 1 / [\alpha(V) + \beta(V)] . \quad (10)$$

The Hodgkin-Huxley equations then become:

$$\begin{aligned} C_m \frac{dV}{dt} &= -g_L (V - E_L) - \bar{g}_{Na} m^3 h (V - E_{Na}) - \bar{g}_K n^4 (V - E_K) \\ \frac{dm}{dt} &= (m_\infty(V) - m) / \tau_m(V) \\ \frac{dh}{dt} &= (h_\infty(V) - h) / \tau_h(V) \\ \frac{dn}{dt} &= (n_\infty(V) - n) / \tau_n(V) , \end{aligned} \quad (11)$$

where m_∞ is the *steady-state activation* and τ_m is the *activation time constant* of the Na^+ current (n_∞ and τ_n represent the same quantities for the K^+ current). In the case of h , h_∞ and τ_h are called *steady-state inactivation* and *inactivation time constant*, respectively. These quantities are important because they can easily be determined from voltage-clamp experiments (see below).

5.2.2 Thermodynamic models

In Hodgkin and Huxley's work, the rate constants $\alpha(V)$ and $\beta(V)$ were fit to the experimental data by using exponential functions of voltage obtained empirically. An alternative approach is to deduce the

exact functional form of the voltage-dependence of the rate constants from thermodynamics. These *thermodynamic models* [7, 8, 9] provide a plausible physical basis to constrain and parameterize the voltage-dependence of rate constants, which are then used to fit voltage-clamp experiments.

Generally, it is assumed that the transition between two states of the channel correspond to a conformational change of the ion channel protein. Consider a transition between an initial (I) and a final (F) state, with a rate constant $r(V)$ that is voltage-dependent:



According to the theory of reaction rates [10, 11], the rate of the transition depends exponentially on the free energy barrier between the two states:

$$r(V) = r_0 e^{-\Delta G(V)/RT} , \quad (13)$$

where r_0 is a constant and $\Delta G(V)$ is the free energy barrier, which can be written as

$$\Delta G(V) = G^*(V) - G_0(V) \quad (14)$$

where $G^*(V)$ is the free energy of an intermediate state (activated complex) state and $G_0(V)$ is the free energy of the initial state, as illustrated in Fig. 1. The relative values of the free energy of the initial and final states (G_0 and G_1) determine the equilibrium distribution between these states, but the kinetics of the transition depend on the size of the free-energy barrier $\Delta G(V)$. Systems with a smaller energy barrier (Fig. 1, dashed line) correspond to faster kinetics because a larger proportion of molecules will have the required energy to form the activated complex and make the transition.

In ion channels, these different states correspond to different conformations of the ion channel protein. How the transition rates between these conformational states depend on membrane potential is given by the voltage-dependence of the free energy barrier, which is in general very difficult to evaluate. The effect of the electrical field on a protein will depend on the number and position of its charged amino-acids, which will result in both linear and nonlinear components in the free energy. Without assumptions about the underlying molecular structure, the free energy of a given state i can be written as a Taylor series expansion of the form:

$$G_i(V) = A_i + B_i V + C_i V^2 + \dots \quad (15)$$

where A_i , B_i , C_i , ... are constants which are specific for each conformational state. The constant A_i corresponds to the free energy that is independent of the electrical field, the linear term $B_i V$ to the interaction between electrical field with isolated charges and rigid dipoles [7, 8, 9, 12]. For example, linear terms in V will result if the conformations differ in their net number of charges, or if

the conformational change is accompanied with the translation of a freely-moving charge inside the structure of the channel [2, 8]. Nonlinear terms results from effects such as electronic polarisation and pressure induced by V [8, 9, 12] or mechanical constraints in the movement of charges due to the structure of the ion channel protein [15].

Thus, each conformational state of the ion channel protein will be associated with a given distribution of charges and will therefore be characterized by a given set of coefficients in Eq. 15. This is also true for the activated state, which is a particular case of conformation. Applying Eqs. 13-15, the rate constant becomes:

$$\begin{aligned} r(V) &= r_0 e^{-[(A^*+B^*V+C^*V^2+\dots)-(A_0+B_0V+C_0V^2+\dots)]/RT} , \\ &= r_0 e^{-(a+bV+cV^2+\dots)/RT} , \end{aligned} \quad (16)$$

where $a = A^* - A_0$, $b = B^* - B_0$, $c = C^* - C_0$, ... represent differences between the linear and nonlinear components of the free energy of the initial and activated states (according to Eq. 15).

Considering the particular case of a reversible open-closed transition



where C and O are respectively the closed and open states, and α and β are the forward and backward rate constants. Applying Eq. 16 to forward and backward reactions leads to the following general expression for the voltage-dependence:

$$\begin{aligned} \alpha(V) &= \alpha_0 e^{-(a_1+b_1V+c_1V^2+\dots)/RT} \\ \beta(V) &= \beta_0 e^{-(a_2+b_2V+c_2V^2+\dots)/RT} \end{aligned} \quad (18)$$

where $a_1, a_2, b_1, b_2, c_1, c_2, \dots$ are constants specific of this transition. It is important to note that, in general, these parameters are not necessary inter-related because the three different conformations implicated here (initial, activated, final, as in Fig. 1) may have very different distributions of charges, resulting in different coefficients in Eq. 15, and thus also resulting in different values for $a_1 \dots c_2$. In the following, this general functional form for the voltage dependence of rate constants will be called *nonlinear thermodynamic model*.

In the “low field limit” (during relatively small transmembrane voltages), the contribution of the higher order terms may be negligible. Thus, a simple, commonly-used voltage dependence results from the first-order approximation of Eqs. 18 and takes the form:

$$\begin{aligned} \alpha(V) &= \alpha_0 e^{-(a_1+b_1V)/RT} \\ \beta(V) &= \beta_0 e^{-(a_2+b_2V)/RT} . \end{aligned} \quad (19)$$

In the following, this form with simple exponential voltage dependence of rate constants will be called *linear thermodynamic model*.

A further simplification is to consider that the conformational change consists of the movement of a gating particle with charge q [1] (see also ref. [13]). The forward and backward rate constants then become:

$$\begin{aligned}\alpha(V) &= \alpha_0 e^{-\gamma q FV/RT} \\ \beta(V) &= \beta_0 e^{(1-\gamma)q FV/RT},\end{aligned}\tag{20}$$

where γ is the relative position of the energy barrier in the membrane (between 0 and 1). The constants α_0 and β_0 can be equated to a fixed constant A by introducing the half-activation voltage V_H , leading to:

$$\begin{aligned}\alpha(V) &= A e^{-\gamma q F(V-V_H)/RT} \\ \beta(V) &= A e^{(1-\gamma)q F(V-V_H)/RT}.\end{aligned}\tag{21}$$

This form was introduced by Borg-Graham [13] for modeling the gating of ion channels. Its parameters are very convenient for fitting experimental data: V_H and q affect the steady-state activation/inactivation curves whereas A and γ only affect the time constant with no effect on steady-state relations.

The drawback of models in which the rate functions are simple exponentials of voltage is that these functions can reach unrealistically high values, which leads to very small time constants and possibly aberrant behavior. A possibility to solve this problem is to force an artificial saturation of the rate constants [14] or impose a minimum value to the time constant [13].

Another possibility is not to limit the approximation of Eqs. 18 to linear terms, but include higher-order terms in the voltage-dependence of the free energy [15]. For example, the quadratic expansion of Eqs. 18 can be written as:

$$\begin{aligned}\alpha(V) &= A e^{-[b_1(V-V_H)+c_1(V-V_H)^2]/RT} \\ \beta(V) &= A e^{[b_2(V-V_H)+c_2(V-V_H)^2]/RT},\end{aligned}\tag{22}$$

and similarly, its cubic expansion:

$$\begin{aligned}\alpha(V) &= A e^{-[b_1(V-V_H)+c_1(V-V_H)^2+d_1(V-V_H)^3]/RT} \\ \beta(V) &= A e^{[b_2(V-V_H)+c_2(V-V_H)^2+d_2(V-V_H)^3]/RT},\end{aligned}\tag{23}$$

where $A, b_1 \dots d_2$ are constants as defined above.

In addition to the effect of voltage on isolated charges or dipoles, described in Eq. 19, these forms account for more sophisticated effects such as the deformation of the protein by the electrical field [8, 9] or mechanical constraints on charge movement [15]. It also gives the possibility for the model to capture more complicated dependence on voltage than the simple exponential functions of Eq. 19, which may result in more realistic behavior (see below).

Finally, another way to impose a minimal value for the time constant is to consider that the gate operates via two successive transitions:



where C_1 and C_2 are two distinct closed states of the gate. The second transition is not dependent of voltage and therefore acts as a rate-limiting factor when α and β are large compared to k_1 and k_2 . In this case, the system will be governed essentially by k_1 and k_2 , which therefore impose a limit on the rate of opening/closure of the gate. On the other hand, when α and β are small compared to k_1 and k_2 , the system will be dominated by the first transition, while the two states C_2 and O will be in rapid quasi-equilibrium. Although this system apparently solves the problem of having a minimal time constant while still conserving the voltage-dependence of the gate, it is nevertheless still unrealistic that the simple exponential representation for α and β permits the first transition to occur arbitrarily fast at some voltages.

Reaction schemes involving multiple states, such as Eq. 24, are reminiscent of another class of models, called *Markov models*, which are described in more detail below.

5.2.3 Markov models

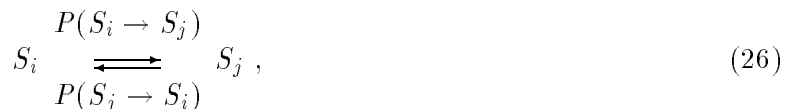
Although the formalism introduced by Hodgkin and Huxley [1] was remarkably forward-looking, and closely reproduced the behavior of macroscopic currents, the advent of single-channel recordings techniques revealed inconsistencies with experimental data. Measurements on Na^+ channels have shown that activation and inactivation must necessarily be coupled [16, 17, 18], which is in contrast with the independence of these processes in the Hodgkin-Huxley model. K^+ channels may also show an inactivation which is not voltage-dependent, as in the Hodgkin-Huxley model, but state-dependent [19]. Although the latter can be modeled with modified Hodgkin-Huxley kinetics [20], these phenomena are best described using Markov models, a formalism more appropriate to describe single channels.

Markov models assume that the gating of a channel occurs through a series of conformational changes of the ion channel protein, and that the transition probability between conformational states depends only on the present state. The sequence of conformations involved in this process can be described by state diagrams of the form:



where $S_1 \dots S_n$ represents distinct conformational states of the ion channel. Defining $P(S_i, t)$ as the probability of being in a state S_i at time t and $P(S_i \rightarrow S_j)$ as the *transition probability* from state S_i

to state S_j , according to:



leads to the following equation for the time evolution of $P(S_i, t)$:

$$\frac{dP(S_i, t)}{dt} = \sum_{j=1}^n P(S_j, t) P(S_j \rightarrow S_i) - \sum_{j=1}^n P(S_i, t) P(S_i \rightarrow S_j). \quad (27)$$

This equation is called the *master equation* (see e.g., refs. [9, 21]). The left term represents the “source” contribution of all transitions entering state S_i , and the right term represents the “sink” contribution of all transition leaving state S_i . In this equation, the time evolution depends only on the present state of the system, and is defined entirely by knowledge of the set of transition probabilities. Such systems are called *Markovian systems*.

In the limit of large numbers of identical channels, the quantities given in the master equation can be replaced by their macroscopic interpretation. The probability of being in a state S_i becomes the *fraction of channels* in state S_i , noted s_i , and the transition probabilities from state S_i to state S_j become the *rate constants*, r_{ij} , of the reactions



In this case, one can rewrite the master equation as:

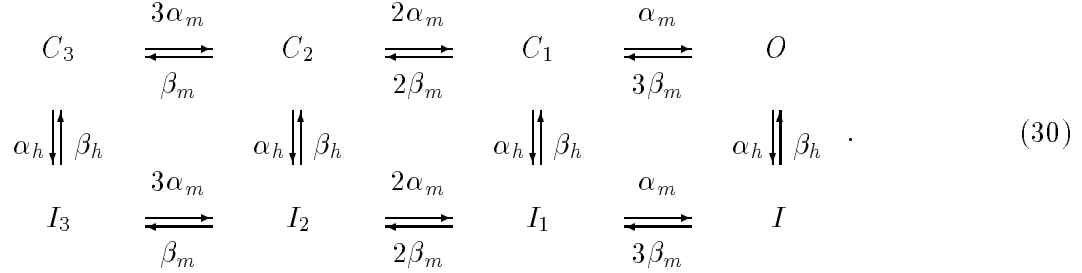
$$\frac{ds_i}{dt} = \sum_{j=1}^n s_j r_{ji} - \sum_{j=1}^n s_i r_{ij}, \quad (29)$$

which is a conventional kinetic equation for the various states of the system.

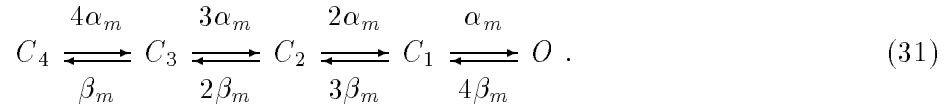
Stochastic Markov models (as in Eq. 27) are adequate to describe the stochastic behavior of ion channels as recorded using single-channel recording techniques (see ref. [5]). In other cases, where a larger area of membrane is recorded and large numbers of ion channels are involved, the macroscopic currents are continuous and more adequately described by conventional kinetic equations, as in Eq. 29 (see ref. [22]). In the following, only systems of the latter type will be considered.

It is to be noted that Markov models are more general than the Hodgkin-Huxley formalism, and include it as a subclass. A Markov scheme can be written for any Hodgkin-Huxley scheme, but the translation of a system with multiple independent gates into a Markov description results in a combinatorial explosion of states. For example, the Markov model corresponding to the Hodgkin-

Huxley sodium channel is [23]:



The states represent the channel with the inactivation gate in the open state (top) or closed state (bottom) and (from left to right) three, two, one or none of the activation gates closed. To be equivalent to the m^3 formulation, the rates must have the 3:2:1 ratio in the forward direction and the 1:2:3 ratio in the backward direction. Only the O state is conducting. The squid delayed rectifier potassium current modeled by Hodgkin and Huxley [1] with 4 activation gates and no inactivation can be treated analogously [23, 24], giving

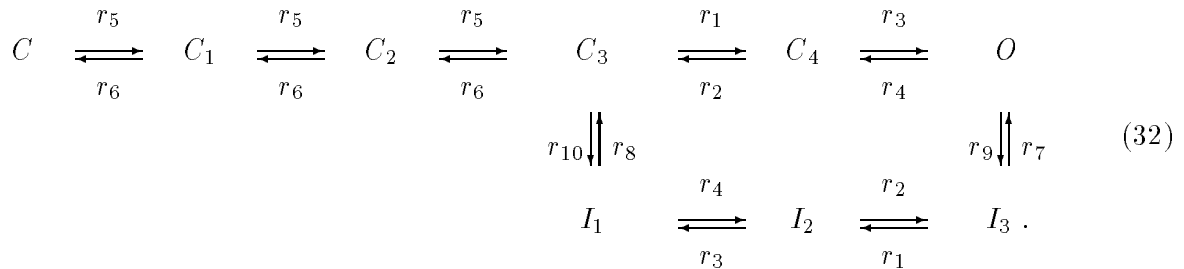


5.3 MODELS TO GENERATE ACTION POTENTIALS

We now use some of the formalisms reviewed above and compare them in similar situations. The voltage-clamp behavior of the sodium channel and the genesis of action potentials are taken as examples to illustrate the differences between these formalisms.

5.3.1 Models of Na^+ and K^+ currents underlying action potentials

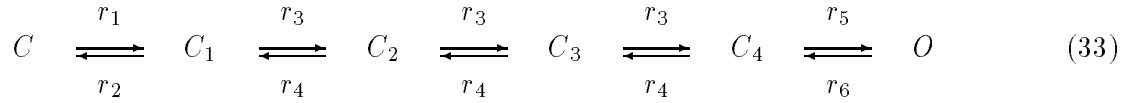
We will compare here the model of Hodgkin and Huxley [1] with two Markov models of Na^+ channels. A nine-state Markov model was proposed by Vandenberg and Bezanilla [25]:



This particular nine-state model was selected to fit not only the measurements of macroscopic ionic currents available to Hodgkin and Huxley, but also recordings of single channel events and measurements of currents resulting directly from the movement of charge during conformational changes of

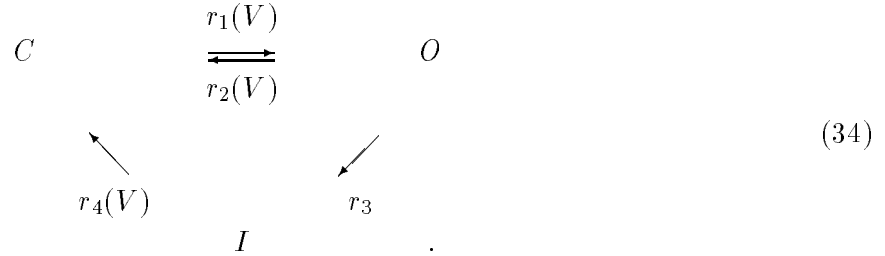
the protein (so-called *gating currents*; see ref. [2]). The voltage-dependence of the transition rates was assumed to be a simple exponential function of voltage (Eqs. 19).

To complement the sodium channel model of Vandenberg and Bezanilla, we also examined the six state scheme for the squid delayed rectifier channel, used by Perozo and Bezanilla [26]:



where again rates were described by a simple exponential function of voltage (Eqs. 19).

The third class of model considered here are simplified Markov models of Na⁺ and K⁺ currents. The model for the Na⁺ channel was chosen to have the fewest possible number of states (three) and transitions (four) while still being capable of reproducing the essential behavior of the more complex models. The form of the state diagram was based on a looped three-state scheme in which some transitions were eliminated, giving an irreversible loop [6, 27]:



This model incorporated voltage-dependent opening, closing, and recovery from inactivation, while inactivation was voltage-independent. For simplicity, neither opening from the inactivated state nor inactivation from the closed state were permitted. Although there is clear evidence for occurrence of the latter [28] it was unnecessary under the conditions of the present simulations. Rate constants were described by

$$r_i(V) = \frac{a_i}{1 + \exp[-(V - c_i)/b]}, \quad (35)$$

with $c_1 = c_2$ to yield a model consisting of nine total parameters [6].

The simplified K⁺ channel model consisted in a single open or conducting state, O , and a single closed state C :



Here, the rates $r_1(V)$ and $r_2(V)$ had a sigmoidal voltage dependence similar to Eq. 35 (see details in ref. [6]).

5.3.2 Na⁺ currents in voltage-clamp

The different types of models reviewed above are characterized by different complexity, ranging from a two-state representation (Eq. 36) to transition diagrams involving many states (Eq. 32). The two-state

description is adequate to fit the behavior of some channels (see refs. [6, 13, 29, 30, 31], but for most channels more complex models must be considered. To illustrate this, we compared three different models of the fast sodium channel underlying action potentials (Figs. 2 and 3).

The response of the three sodium channel models were compared during a voltage-clamp step from rest (-75 mV) to a depolarized level of -20 mV (Fig. 2). For all three models, the closed states were favored at hyperpolarized potentials. Upon depolarization, forward (opening) rates sharply increased while closing (backward) rates decreased, causing a migration of channels in the forward direction toward the open state. The three closed states in the Hodgkin-Huxley model and the five closed states in the Vandenberg-Bezanilla model gave rise to the characteristic delayed activation and sigmoidal shape of the rising phase of the sodium current (Fig. 2D). In contrast, the simple model, with a single closed state, produced a first-order exponential response to the voltage step and was therefore not sigmoidal.

These models generate different predictions about single-channel behavior. The steady-state behavior of the Hodgkin-Huxley model of the macroscopic sodium current is remarkably similar to that of the model of Vandenberg and Bezanilla [25], but there are important differences in the relationship between activation and inactivation. First, in the Hodgkin-Huxley model, activation and inactivation are kinetically independent. This independence has been shown to be untenable on the basis of gating and ion current measurements in the squid giant axon [16, 17, 18]. Consequently, Markov models that reproduce gating currents, such as the Vandenberg-Bezanilla model examined here, require schemes with coupled activation and inactivation. Likewise, in the simple model, activation and inactivation were strongly coupled due to the unidirectional looped scheme (Eq. 34), so that channels were required to open before inactivating and could not reopen from the inactivated state before closing.

A second difference is that, in the Hodgkin-Huxley and Vandenberg-Bezanilla models, inactivation rates are slow and activation rates fast. In the simplified Markov model, the situation was reversed, with fast inactivation and slow activation. At the macroscopic level modeled here, these two relationships gave rise to similar times course for open channels (Fig. 2A-C; see ref. [12]). However, the two classes of models make distinct predictions for single-channel behavior. Whereas the Hodgkin-Huxley and Vandenberg-Bezanilla models predict the latency to first channel opening to be short and channel open times to be comparable to the time course of the macroscopic current, the simplified Markov model predicts a large portion of first channel openings to occur after the peak of the macroscopic current and to have open times much shorter than its duration.

5.3.3 Genesis of action potentials

Despite the significant differences in their complexity and formulation, the three models of the sodium channel all produced very comparable action potentials and repetitive firing when combined with

appropriate delayed-rectifier potassium channel models (Fig. 3). These simulations thus seem to perform similarly for fitting the macroscopic behavior of Na^+ and K^+ currents.

However, these three models generated clear differences when compared in voltage-clamp (Fig. 2) and still larger differences would be expected at the single-channel level. Thus, which model to choose clearly depends on the scope of the model. If the detailed behavior of voltage-clamp experiments or single-channel recordings are to be reproduced, Markov models are certainly the most appropriate representation. However, if the goal is to reproduce the qualitative features of membrane excitability, action potentials and repetitive firing, all models seem equivalent, except that simpler models are faster to compute. Thus in this case, simplified two- or three-state schemes or the Hodgkin-Huxley model would seem most appropriate.

5.4 FITTING MODELS TO VOLTAGE-CLAMP DATA

The different formalisms reviewed above are now applied to a concrete example of voltage-clamp experiments. We consider the T-type (“low-threshold”) calcium current responsible for bursting behavior in thalamic neurons [32].

5.4.1 Voltage-clamp characterization of the T-current

Whole-cell voltage-clamp recordings of the T-type calcium current were obtained from thalamic relay neurons acutely dissociated from the ventrobasal thalamus of young rats (P8-P15). All voltage-clamp recordings were at a temperature of 24°C . The Methods were described in detail in ref. [33].

The T-current is transient and has activation/inactivation characteristics similar to the Na^+ current, but is slower and its voltage range for activation/inactivation typically occurs around rest. These properties are illustrated in Fig. 4. A series of voltage steps from a hyperpolarized level (-100 mV) to various depolarized levels reveal an inward current that activates and inactivates in a voltage-dependent manner (Fig. 4A1). Interrupting this protocol before complete inactivation generates tail currents (Fig. 4A2) which reveal the de-activation characteristics of the current.

The fitting of these current traces was performed as follows. The most optimal template (determined by difference in residuals) included two activation gates and one inactivation gate, leading to the m^2h format in Hodgkin-Huxley equations [33]. To measure activation, the influence of inactivation must be as minimal as possible. We assumed that activation is essentially complete in 10 ms, and that there is negligible inactivation (these assumptions were checked by calculating the expected activation and inactivation at various voltages). We used the amplitude of the tail current, which reflects the number of channels open at the end of the depolarizing step, as a measure of activation (m^2). The values obtained using this procedure were very close to those obtained by fitting Hodgkin-Huxley

equations to current traces [33]. The advantage of the tail current approach is that the driving force is the same for all measurements, therefore providing a direct measure of normalized conductance. This type of procedure leads to estimates of steady-state activation (Fig. 4B). The time constants were estimated by fitting exponential templates to the current traces (Fig. 4C; see Methods in ref. [34]).

The inactivation characteristics of I_T are shown in Fig. 5. A series of holding potentials given at various voltages, before applying a command potential at -30 mV, shows different current traces which contain similar activation but different levels of inactivation (Fig. 5A1). A particular feature of the T-current is that the recovery from inactivation is very slow (Fig. 5A2). Estimated steady-state relations for several cells using similar protocols are shown in Fig. 5B and the time constants are shown in Fig. 5C.

Thus the T-current in thalamic relay neurons has activation and inactivation which are characterized by relatively slow time constants, and a slow recovery from inactivation, almost an order of magnitude slower than inactivation. In the following, we examine different representations to model the behavior of this current.

5.4.2 Hodgkin-Huxley model of the T-current

The voltage-clamp behavior shown above was first modeled by a Hodgkin-Huxley type representation in which rate constants were fit to experimental data using empirical functions of voltage [34]. Due to the nonlinear behavior of calcium currents (the internal and external Ca^{2+} concentration differ by about four orders of magnitude), they were represented using the constant-field equations (also called Goldman-Hodgkin-Katz equations; see ref. [2]; for implementation, see ref. [35]):

$$I_T = \bar{P}_{Ca} m^2 h G(V, Ca_o, Ca_i) \quad (37)$$

where \bar{P}_{Ca} (in cm/s) is the maximum permeability of the membrane to Ca^{2+} ions and $G(V, Ca_o, Ca_i)$ is a nonlinear function of voltage and ionic concentrations:

$$G(V, Ca_o, Ca_i) = Z^2 F^2 V / RT \frac{Ca_i - Ca_o \exp(-ZFV/RT)}{1 - \exp(-ZFV/RT)} \quad (38)$$

where $Z=2$ is the valence of calcium ions. Ca_i and Ca_o are the intracellular and extracellular Ca^{2+} concentrations (in M), respectively.

The variables m and h represent respectively the activation and inactivation variables and obey first-order equations similar to Eq. 8. Their steady-state relations were fit using Boltzmann functions (Fig. 6A-B, blue curves), leading to the following optimal functions:

$$\begin{aligned} m_\infty(V) &= 1 / (1 + \exp[-(V + 57)/6.2]) \\ h_\infty(V) &= 1 / (1 + \exp[(V + 81)/4]) \end{aligned}$$

Similarly, the voltage-dependent time constants were estimated by fitting exponential functions to the values determined experimentally (Fig. 6C-D, blue curves), leading to the following expression for activation:

$$\tau_m(V) = 0.612 + 1 / (\exp[-(V + 132)/16.7] + \exp[(V + 16.8)/18.2]) \quad (39)$$

and for inactivation:

$$\begin{aligned} \tau_h(V) = & 28 + \exp[-(V + 22)/10.5] & \text{for } V \geq -81 \text{ mV} \\ & \exp[(V + 467)/66.6] & \text{for } V < -81 \text{ mV} \end{aligned} \quad (40)$$

Here two different functions were fit to the time constants τ_h obtained from inactivation protocols ($V \geq -81$) or recovery from inactivation ($V < -81$).

The temperature dependence of these empirical functions was adjusted according to the following rule:

$$\tau' = \tau Q_{10}^{-(T-24)/10}, \quad (41)$$

where Q_{10} is the experimentally-determined change of time constants for a 10-degree difference in temperature. For the T-current in thalamic neurons, Q_{10} was determined as equal to 5 for τ_m and 3 for τ_h [36].

The behavior of this model is shown in Fig. 7A. The model accounted well for all protocols of Figs. 4 and 5, with activation and recovery from inactivation shown in Fig. 7A1 and A2, respectively. However, in this model, τ_m and τ_h were fit using functions of voltage obtained empirically. Similar to the work of Hodgkin and Huxley [1], this approach leads to a model that accounts well for the current-clamp behavior of the T-current in thalamic neurons [37] (see below).

5.4.3 Linear thermodynamic model of the T-current

Another possibility is to deduce the functional form of rate constants from thermodynamic arguments. The first of such models is the linear approximation (Eqs. 19), which corresponds to the same equations as Eqs. 37 above, but with a functional form dictated by a linear voltage-dependence of the free energy barrier. Constraining the fitting using rate constants described by Eqs. 19 (Fig. 6, green curves) led to the following optimal expressions:

$$\alpha_m = 0.049 \exp[444 \gamma_m (V + 54.6)/RT] \quad (42)$$

$$\beta_m = 0.049 \exp[-444 (1 - \gamma_m) (V + 54.6)/RT] \quad (43)$$

$$\alpha_h = 0.00148 \exp[-559 \gamma_h (V + 81.9)/RT] \quad (44)$$

$$\beta_h = 0.00148 \exp[559 (1 - \gamma_h) (V + 81.9)/RT] \quad (45)$$

where $\gamma_m=0.90$ and $\gamma_h=0.25$. The steady-state relations and time constants are obtained similarly as Eqs. 9-10.

This model provided a good fit of the steady-state relations (Fig. 6A-B, green curves) but the fit to time constants was poor (Fig. 6C-D, green curves). In particular, it was not possible to capture the saturation of τ_m and τ_h to constant values for depolarized membrane potentials. This poor fit had catastrophic consequences, as illustrated in Fig. 7B. Due to the near-zero time constants at depolarized levels, the current activated and inactivated too fast and led to peak current amplitudes that were over an order of magnitude smaller than the Hodgkin-Huxley model at same channel densities (compare A and B in Fig. 7). We conclude that linear thermodynamic models do not provide an acceptable behavior in voltage-clamp for the T-current.

A possibility to resolve this inherent limitation is to add an artificial minimum value to the time constant [13], but this possibility was not considered here in order to stay within a physically-plausible formalism. Instead, we illustrate below that this problem can be solved by including higher-order voltage-dependent contributions in the free energy barrier [15].

5.4.4 Nonlinear thermodynamic model of the T-current

Nonlinear thermodynamic models assume that the free energy barrier depends nonlinearly on voltage (see Eqs. 18) and that each conformational state involved has its own dependence on voltage, independently of other conformational states [15]. The consequence is that the coefficients $a_1 \dots c_2$ in Eqs. 18 can take any value independently of each other. Using these nonlinear expressions to fit the voltage-clamp data of the T-current led to better fits of T-channel data. The quadratic expansion still provided a poor fit of the time constants, although better than linear fits (not shown). Acceptable fits were obtained for a cubic expansion of the rate constants, given by:

$$\begin{aligned}
 \alpha_m(V) &= A_m \exp [b_{m1} (V - V_m) + c_{m1} (V - V_m)^2 + d_{m1} (V - V_m)^3] / RT \\
 \beta_m(V) &= A_m \exp [b_{m2} (V - V_m) + c_{m2} (V - V_m)^2 + d_{m2} (V - V_m)^3] / RT \\
 \alpha_h(V) &= A_h \exp - [b_{h1} (V - V_h) + c_{h1} (V - V_h)^2 + d_{h1} (V - V_h)^3] / RT \\
 \beta_h(V) &= A_h \exp [b_{h2} (V - V_h) + c_{h2} (V - V_h)^2 + d_{h2} (V - V_h)^3] / RT .
 \end{aligned} \tag{46}$$

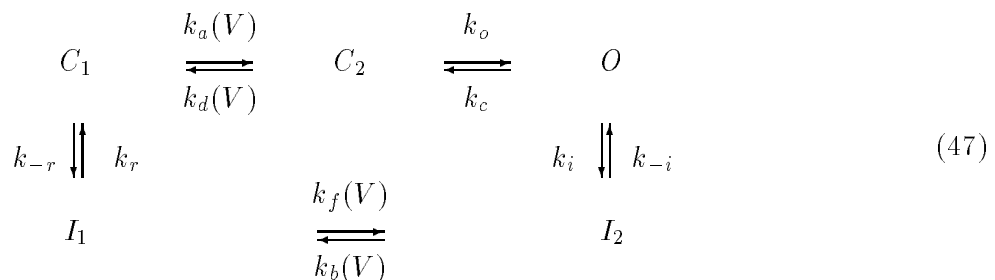
The best fit of this nonlinear thermodynamic model is shown in Fig. 6 (red curves) and was obtained with the following parameters: $A_m = 0.053 \text{ ms}^{-1}$, $V_m = -56 \text{ mV}$, $b_{m1} = -260$, $c_{m1} = 2.20$, $d_{m1} = 0.0052$, $b_{m2} = 64.85$, $c_{m2} = 2.02$, $d_{m2} = 0.036$, $A_h = 0.0017 \text{ ms}^{-1}$, $V_h = -80 \text{ mV}$, $b_{h1} = 163$, $c_{h1} = 4.96$, $d_{h1} = 0.062$, $b_{h2} = -438$, $c_{h2} = 8.73$, $d_{h2} = -0.057$. Fig. 6 (red curves) shows that this model could capture the form of the voltage-dependence of the time constants. In particular, it could fit the saturating values for the time constants at depolarized level, in a manner similar to the empirical functions used for the Hodgkin-Huxley type model (Fig. 6, blue curves). Nonlinear expansions of higher order provided better fits, but the difference was not qualitative (not shown).

Using these rate constants with Eqs. 37 produced acceptable voltage-clamp behavior, as shown in

Fig. 7C. All protocols of activation (Fig. 7C1), deactivation (not shown), inactivation (not shown), and recovery from inactivation (Fig. 7C2) showed a similar voltage-dependent behavior as the experimental data.

5.4.5 Markov model of the T-current

To illustrate the Markov representation, we have used a model of the T-current introduced by Chen and Hess [38]. This model was obtained based on voltage-clamp recordings and single-channel recordings of the T-current in fibroblasts, and the following optimal scheme was proposed [38]:



Here, only k_a , k_d , k_f and k_b are voltage-dependent while the other rates are constant. Thus, activation occurs through one voltage-dependent step (k_a , k_d) and one voltage-independent step (k_o , k_c), the latter being rate-limiting if k_a and k_d reach high values. Similarly, the inactivation occurs first through a voltage-independent step (k_i , k_{-i}), followed by a voltage-dependent transition (k_f , k_b) and a voltage-independent return to the closed state (k_r , k_{-r}).

Fitting the parameters of Markov models to experimental data is in general difficult. It is not possible to obtain an analytic expression for both time constants and steady-state relations due to the too high complexity of the model. In general, the activation and inactivation will be described by multiexponential processes with several time constants, and how to relate these multiple time constants with the time constants estimated from experimental data (Figs. 4-5) is not trivial. Rather, the parameters of Markov models are deduced from various experimental considerations (see below). It is also possible to directly fit the Markov model to the original voltage clamp traces, by minimizing the error between the model and *all* experimental traces. Although in principle more accurate, this procedure is difficult to realize in practice because of the complexity of the model (11 parameters here).

The choice of these parameters was guided by the following considerations [38]: (a) the value of k_i must be close to the saturating value of the rate of inactivation at depolarized membrane potentials (Fig. 5C), and k_{-i} must be much smaller to insure complete inactivation; (b) k_c must be close to the fastest activation time constants at negative potentials (Fig. 4C), while k_o must be large ($>1 \text{ ms}^{-1}$) to be compatible with the short bursts of opening in single-channel recordings [38]; (c) the sum $k_r + k_{-r}$ determines the rate of recovery from inactivation at negative membrane potentials; (d) the values

of k_a and k_d were adjusted to obtain the best fit to activation/inactivation voltage-clamp recordings using a thermodynamic template with a linear dependence of the free-energy on voltage:

$$k = k_0 \exp(qFV/RT) \quad (48)$$

where $q = 3.035$ is the net charge of a gating particle. As this scheme is cyclic, microscopic reversibility imposes that the clockwise product of rate constants equals the anticlockwise product, which in turn imposes that the voltage-dependence of k_f and k_b must be the same as that of k_a and k_d . The optimal values of the rate constants were (all units are ms^{-1}):

$$\begin{aligned} k_a &= 6.4 \exp[qF(V-s)/RT] \\ k_d &= 0.000502 \exp[-qF(V-s)/RT] \\ k_f &= 16 \exp[qF(V-s)/RT] \\ k_b &= 2 \times 10^{-6} \exp[-qF(V-s)/RT] \\ k_o &= 3 \\ k_c &= 0.7 \\ k_i &= 0.036 \\ k_{-i} &= 8 \times 10^{-5} \\ k_r &= 0.001 \\ k_{-r} &= 0.003 \end{aligned} \quad (49)$$

Here, the parameters were adapted to recordings of the T-current in thalamic neurons. An additional parameter, $s = -5$ mV, was introduced to shift the voltage-dependence to adjust the model to the thalamic T-current.

Simulation of this model was performed with the above expressions for rate constants, and the T-current described by the following equation:

$$I_T = \bar{P}_{C_a} [O] G(V, C a_o, C a_i) \quad (50)$$

where $[O]$ is the fraction of channels in the open state. Simulated voltage-clamp experiments (Fig. 7D) show that the Chen & Hess model reproduced well the activation characteristics of the T-current (Fig. 7D1) as well as its slow recovery from inactivation (Fig. 7D2). However, this model did not fit quantitatively the T-current of thalamic neurons, because it was based on single-channel recordings of the T-current in fibroblasts, which is different than the “neuronal” T-current (see analysis in ref. [38]). Obtaining a better Markov representation of the thalamic T-current would require to constrain the model by single-channel recordings.

5.4.6 Comparison of the different models

The different models reviewed above for the T-current were compared in current-clamp. A single compartment model of the TC cell was generated (same parameters as in ref. [39]) and contained leak currents and the T-current according to the following equation:

$$C_m \frac{dV}{dt} = -g_L (V - E_L) - I_T, \quad (51)$$

where $C_m=0.88\mu\text{F}/\text{cm}^2$ is the membrane capacitance, $g_L=0.038\text{ mS}/\text{cm}^2$ and $E_L=-77\text{ mV}$ are the leak conductance and reversal potential, and I_T is the T-current as given by Eq. 37. These parameters were obtained by matching the model to thalamic neurons recorded *in vitro* [39].

Using this model, the genesis of low-threshold spike (LTS) was monitored through return to rest after injecting hyperpolarizing currents. The empirical Hodgkin-Huxley type model of the T-current generated LTS in a grossly all-or-none fashion (Fig. 8A). The linear thermodynamic model (Fig. 8B) did not generate LTS, consistent with the very small amplitude of the current evidenced above (Fig. 7B). On the other hand, the nonlinear thermodynamic model (Fig. 8C) and the Markov model of the T-current (Fig. 8D) presented a behavior more consistent with the Hodgkin-Huxley type model. The peak amplitude of the LTS was compared between different models in Fig. 8E. Although the shape of the LTS were not identical, Hodgkin-Huxley and nonlinear thermodynamic models produced remarkably similar peak amplitudes (filled circles and triangles in Fig. 8E). We therefore conclude that nonlinear thermodynamic models provide fits of comparable quality to empirical Hodgkin-Huxley models, but their form is physically more plausible.

5.5 CONCLUSION

In this chapter, we have compared different representations for modeling voltage-dependent currents and delineated some of the differences between these representations. In the case of sodium channels, models of increasing complexity, from simplified two-state representations to multistate Markov diagrams, can capture some of the features of sodium channels and of action potentials. Which model to chose depends on the type of experimental data available and its level of precision. It is clear that a two-state scheme cannot capture the features of single-channel recordings, which require Markov models of sufficient complexity to account for the data. On the other hand, we showed that even simplified two- or three-state representations can capture phenomena such as action potentials [6]. If the principal requirement is to generate action potentials, it is therefore not necessary to include all the complexity of the most sophisticated Markov diagrams of channels and simplified representations appears sufficient. This simplistic approach may be adequate for models involving large-scale networks

of thousands of cells, for which computational efficiency is a more important concern than reproducing all the microscopic features of the channels.

In the case of the T-current, we have shown that various formalisms, such as empirical Hodgkin-Huxley type models, thermodynamic models and Markov models, can capture the behavior of the T-current in voltage-clamp and generate low-threshold spikes. In this case, Markov models are probably more accurate because they also account for single-channel recordings, while Hodgkin-Huxley type models do not. The voltage-clamp data shown here were obtained in thalamic neurons [33] and, for the particular case of these data, they were best modeled by a Hodgkin-Huxley type model in which rate constants were fit to experimental data using empirical functions of voltage. The best physically-plausible approach to capture these data is to use templates taken from nonlinear thermodynamic models, which provide a fitting of comparable quality to empirical functions (compare blue and red curves in Fig. 6). We therefore conclude that nonlinear thermodynamic models should be used to yield representations that are consistent with experimental data while having a plausible biophysical interpretation.

References

- [1] Hodgkin AL and Huxley AF (1952) A quantitative description of membrane current and its application to conduction and excitation in nerve. *J. Physiol.* **117**, 500-544.
- [2] Hille B (1992) *Ionic Channels of Excitable Membranes*. Sinauer Associates INC, Sunderland, MA.
- [3] Armstrong CM and Hille B (1998) Voltage-gated ion channels and electrical excitability. *Neuron* **20**, 371-380.
- [4] Llinás RR (1988) The intrinsic electrophysiological properties of mammalian neurons: a new insight into CNS function. *Science* **242**, 1654-1664.
- [5] Sakmann B and Neher E (Editors) (1995) *Single-Channel Recording* (2nd edition). Plenum Press, New York, NY.
- [6] Destexhe A, Mainen ZF and Sejnowski TJ (1994) Synthesis of models for excitable membranes, synaptic transmission and neuromodulation using a common kinetic formalism. *J. Computational Neuroscience* **1**, 195-230.
- [7] Tsien RW and Noble D (1969) A transition state theory approach to the kinetics of conductances in excitable membranes. *J. Membr. Biol.* **1**, 248-273.

- [8] Hill TL and Chen YD (1972) On the theory of ion transport across nerve membranes. VI. Free energy and activation free energies of conformational change. *Proc. Natl. Acad. Sci. USA* **69**, 1723-1726.
- [9] Stevens CF (1978) Interactions between intrinsic membrane protein and electric field. *Biophys. J.* **22**, 295-306.
- [10] Eyring H (1935) The activated complex in chemical reactions. *J. Chem. Phys.* **3**, 107-115.
- [11] Johnson FH, Eyring H and Stover BJ (1974) *The theory of rate processes in biology and medicine*, John Wiley and Sons, New York.
- [12] Andersen O and Koeppe RE II (1992) Molecular determinants of channel function. *Physiol. Rev.* **72**, S89-S158.
- [13] Borg-Graham LJ (1991) Modeling the nonlinear conductances of excitable membranes. In: Wheal H and Chad J, eds. *Cellular and Molecular Neurobiology: A Practical Approach*. Oxford University Press, New York, pp. 247-275.
- [14] Willms AR, Baro DJ, Harris-Warrick RM and Guckenheimer J. (1999) An improved parameter estimation method for Hodgkin-Huxley models. *J. Comput. Neurosci.* **6**, 145-168.
- [15] Destexhe A and Huguenard JR (2000) Nonlinear thermodynamic models of voltage-dependent currents. *J. Computational Neuroscience* (submitted).
- [16] Armstrong CM (1981) Sodium channels and gating currents. *Physiol. Rev.* **62**, 644-683.
- [17] Aldrich RW, Corey DP and Stevens CF (1983) A reinterpretation of mammalian sodium channel gating based on single channel recording. *Nature* **306**, 436-441.
- [18] Bezanilla F (1985) Gating of sodium and potassium channels. *J. Membr. Biol.* **88**, 97-111.
- [19] Aldrich RW (1981) Inactivation of voltage-gated delayed potassium currents in molluscan neurons. *Biophys. J.* **36**, 519-532.
- [20] Marom S and Abbott LF (1994) Modeling state-dependent inactivation of membrane currents. *Biophys. J.* **67**, 515-520.
- [21] Colquhoun D and Hawkes AG (1981) On the stochastic properties of single ion channels. *Proc. Roy. Soc. Lond. Ser. B* **211**, 205-235.
- [22] Johnston D and Wu SM (1995) *Foundations of Cellular Neurophysiology*. MIT Press, Cambridge, MA.

- [23] Fitzhugh R (1965) A kinetic model of the conductance changes in nerve membrane. *J. Cell. Comp. Physiol.* **66**, 111-118.
- [24] Armstrong CM (1969) Inactivation of the potassium conductance and related phenomena caused by quaternary ammonium ion injection in squid axons. *J. Gen. Physiol.* **54**, 553-575.
- [25] Vandenberg CA and Bezanilla F (1991) A model of sodium channel gating based on single channel, macroscopic ionic, and gating currents in the squid giant axon. *Biophys. J.* **60**, 1511-1533.
- [26] Perozo E and Bezanilla F (1990) Phosphorylation affects voltage gating of the delayed rectifier K⁺ channel by electrostatic interactions. *Neuron* **5**, 685-690.
- [27] Bush P and Sejnowski TJ (1991) Simulations of a reconstructed cerebellar Purkinje cell based on simplified channel kinetics. *Neural Computation* **3**, 321-332.
- [28] Horn RJ, Patlak J and Stevens CF (1981) Sodium channels need not open before they inactivate. *Nature* **291**, 426-427.
- [29] Labarca P, Rice JA, Fredkin DR and Montal M (1985) Kinetic analysis of channel gating. Application to the cholinergic receptor channel and the chloride channel from *Torpedo Californica*. *Biophys. J.* **47**, 469-478.
- [30] Yamada WN, Koch C and Adams PR (1989) Multiple channels and calcium dynamics. In: C Koch and I Segev, eds., *Methods in Neuronal Modeling*. Cambridge, MA: MIT Press, pp. 97-134.
- [31] Destexhe A, Mainen ZF and Sejnowski TJ (1998) Kinetic models of synaptic transmission. In: *Methods in Neuronal Modeling* (2nd edition) (ed. Koch C and Segev I), MIT Press, Cambridge, MA, pp. 1-26.
- [32] Jahnsen H, Llinás RR (1984) Ionic basis for the electroresponsiveness and oscillatory properties of guinea-pig thalamic neurons *in vitro*. *J. Physiol.* **349**, 227-247.
- [33] Huguenard JR and Prince DA (1992) A novel T-type current underlies prolonged calcium-dependent burst firing in GABAergic neurons of rat thalamic reticular nucleus. *J. Neurosci.* **12**, 3804-3817.
- [34] Huguenard JR and McCormick DA (1992) Simulation of the currents involved in rhythmic oscillations in thalamic relay neurons. *J. Neurophysiol.* **68**, 1373-1383.
- [35] De Schutter E and Smolen P (1998) Calcium dynamics in large neuronal models. In: *Methods in Neuronal Modeling* (2nd edition) (ed. Koch C and Segev I), MIT Press, Cambridge, MA, pp. 211-250.

- [36] Coulter DA, Huguenard JR and Prince DA (1989) Calcium currents in rat thalamocortical relay neurones: kinetic properties of the transient, low-threshold current. *J. Physiol.* **414**: 587-604.
- [37] McCormick DA and Huguenard JR (1992) A model of the electrophysiological properties of thalamocortical relay neurons. *J. Neurophysiol.* **68**, 1384-1400.
- [38] Chen C and Hess P (1990) Mechanisms of gating of T-type calcium channels. *J. Gen. Physiol.* **96**, 603-630.
- [39] Destexhe A, Neubig M, Ulrich D and Huguenard JR (1998) Dendritic low-threshold calcium currents in thalamic relay cells. *J. Neurosci.* **18**, 3574-3588.

Gate	Forward rate constant	Backward rate constant
m	$\alpha_m = \frac{-0.1 (V - V_r - 25)}{\exp[-(V - V_r - 25)/4] - 1}$	$\beta_m = 4 \exp[-(V - V_r)/18]$
h	$\alpha_h = 0.07 \exp[-(V - V_r)/20]$	$\beta_h = \frac{1}{1 + \exp[-(V - V_r + 30)/10]}$
n	$\alpha_n = \frac{-0.01 (V - V_r + 10)}{\exp[-(V - V_r + 10)/10] - 1}$	$\beta_n = 0.125 \exp[-(V - V_r)/80]$

Table 1: Rate constants of the Hodgkin-Huxley model.

The rate constants are given for the variables m , n , h as in Eq. 7. The rate constants are those estimated by Hodgkin and Huxley [1] in squid giant axon at a temperature around $6^\circ C$. In the original study, the voltage axis was reversed in polarity and voltage values were given with respect to the resting membrane potential (V_r here).

Figure 1:

Schematic representation of the free energy profile of conformational changes in ion channels. The diagram represents the free energy of different states involved in a transition: the initial state, activated complex and final state. The equilibrium distribution between initial and final states depends on the relative value of their free energy (G_0 and G_1). The rate of the transition will be governed by the *free energy barrier* ΔG , which is the free energy difference between the activated complex and the initial state. If the energy barrier is smaller (dashed line), the kinetics of the reaction is faster because a larger proportion of ion channels will have the required energy to make the transition. Figure modified from ref. [15].

Figure 2:

Three kinetic models of a squid axon sodium channel produce qualitatively similar conductance time courses. A voltage-clamp step from rest, $V = -75 \text{ mV}$, to $V = -20 \text{ mV}$ was simulated. The fraction of channels in the open state (O , thick solid line), closed states (C , thick dashed lines), and inactivated states (I , thick dotted lines) are shown for the Hodgkin-Huxley model [1], a detailed markov model [25], and a simple Markov model [6]. A. Hodgkin-Huxley model of the sodium channel (Eq. 30). The activation (m) and inactivation (h) gates were deduced from other states and are indicated by thin lines. B. Markov model of Vandenberg and Bezanilla [25] (Eq. 32). Individual closed and inactivated states are shown (thin lines), as well as the sum of all 5 closed states (C), the sum of all 3 inactivated states (I) and the open state (O). C. Simplified three-state Markov model [6] (Eq. 34). D. Comparison of the time course of open channels for the three models on a faster time scale shows differences immediately following the voltage step. The Hodgkin-Huxley (H-H) and Vandenberg-Bezanilla (V-B) models give smooth, multiexponential rising phases, while the three-state Markov model (Simple) gives a single exponential rise with a discontinuity in the slope at the beginning of the pulse. Figure modified from ref. [6]; parameters given in the CD-ROM.

Figure 3:

Similar action potentials produced using three different kinetic models of squid fast sodium and delayed rectifying potassium channels. A. Single action potentials in response to 0.2 ms , 2 nA current pulse are elicited at similar thresholds and produce similar waveforms using three different pairs of kinetic models: Hodgkin-Huxley [1] (dashed line), detailed Markov models [25, 26] (dotted line), and simplified kinetic models (solid line). B. Repetitive trains of action potentials elicited in response to sustained current injection (0.2 nA) have slightly different frequencies. Sodium channels were modeled as described in Fig. 2. The detailed Markov potassium channel model had 6 states [26] (Eq. 33) and the simple model of potassium channel had 2 states (Eq. 36). Figure modified from ref. [6]; parameters given in the CD-ROM.

Figure 4:

Voltage-clamp recordings of the T-current in dissociated thalamic relay neurons. A. Voltage-clamp protocols for activation (A1) and deactivation (A2). Command potentials at various levels were given after the cell was maintained at a hyperpolarized holding potential, leading to the activation of the current. B. Steady-state activation obtained from the tail currents in A2, which were fit to a m^2h template. C. Time constants obtained using a similar procedure. Different symbols correspond to different cells. Figure modified from ref. [34] where all details were given.

Figure 5:

Voltage-clamp characterization of T-current inactivation in dissociated thalamic relay neurons. A. Voltage-clamp protocols for inactivation (A1) and recovery from inactivation (A2). In A1, the cell was maintained at different holding potentials then stepped to -30 mV to activate the T-current with different levels of inactivation. In A2, the current is reactivated after being fully inactivated. The full recovery took about 1 second (recovery time constant of about 300 ms). B. Steady-state inactivation calculated by the peak of currents in A1. C. Inactivation time constants obtained by fitting a m^2h template to the data. The recovery time constants were obtained by fitting a single-exponential to the recovery experiment (dashed line in A2). Different symbols correspond to different cells. Figure modified from ref. [34] where all details were given.

Figure 6:

Fitting of different models to the T-current in thalamic relay neurons. In each panel, the symbols show the voltage-clamp data obtained in several thalamic neurons (see Figs. 4-5) and the continuous curves show the best fits obtained with an empirical Hodgkin-Huxley type model (blue), a linear thermodynamic model (green) and a nonlinear thermodynamic model (red). A. Steady-state activation (m_∞^2). B. Steady-state inactivation (h_∞). C. Activation time constant (τ_m). D. Inactivation time constant (τ_h). The leftmost symbols in D (≤ -80 mV) are the data from the slow recovery from inactivation of the T-current. See text for the values of the parameters. All functions were fit using a simplex method (see Chapter 1). Figure modified from ref. [15].

Figure 7:

Voltage-clamp behavior of different models of the T-current. Left panels: activation protocol (identical to Fig. 4A1); right panels: protocol for the recovery from inactivation (identical to Fig. 5A2). A. Empirical Hodgkin-Huxley type model. B. Linear thermodynamic model. C. Nonlinear thermodynamic model. D. Markov model. In all cases, the same density of T-channels was used ($\bar{P}_{Ca} = 3 \times 10^{-6}$ cm/s). Figure modified from ref. [15].

Figure 8:

Low-threshold spikes generated by different models of the T-current. Comparison of the same current-clamp simulation for 4 different models of the T-current: an empirical Hodgkin-Huxley type model (A), a linear thermodynamic model (B), a nonlinear thermodynamic model (C) and a Markov model (D). The simulation consisted in injecting hyperpolarizing current pulses of various amplitudes (-0.025, -0.05, -0.075, -0.1, -0.125 and -0.15 nA) and of 1 sec duration. At the end of the pulse, the model generated a low-threshold spike upon return to rest. E. Peak amplitude of low-threshold spikes (LTS) generated by the different models of the T-current. All simulations were done with the same single-compartment geometry which contained leak currents in addition to the T-current (identical parameters as in ref. [39]). The density of T-channels was identical in all cases ($\bar{P}_{Ca} = 5 \times 10^{-5}$ cm/s) and was in the range of densities estimated from rat ventrobasal thalamic neurons [39]. Figure modified from ref. [15].

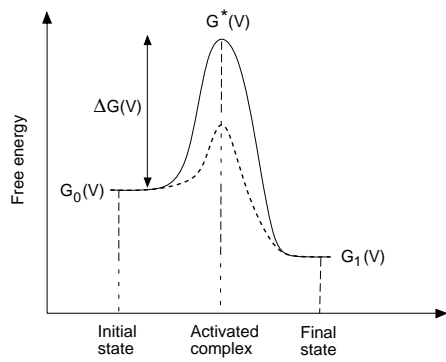


Fig. 1

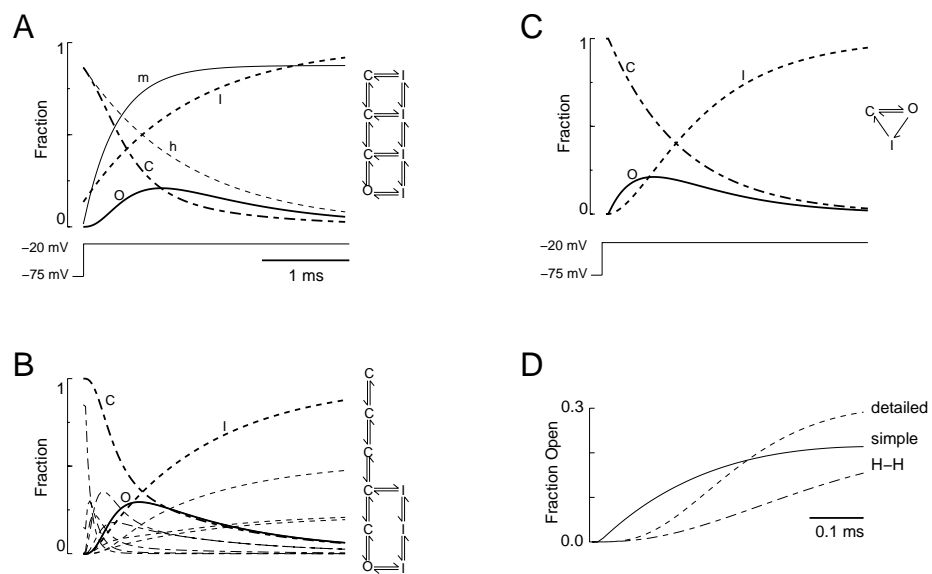


Fig. 2

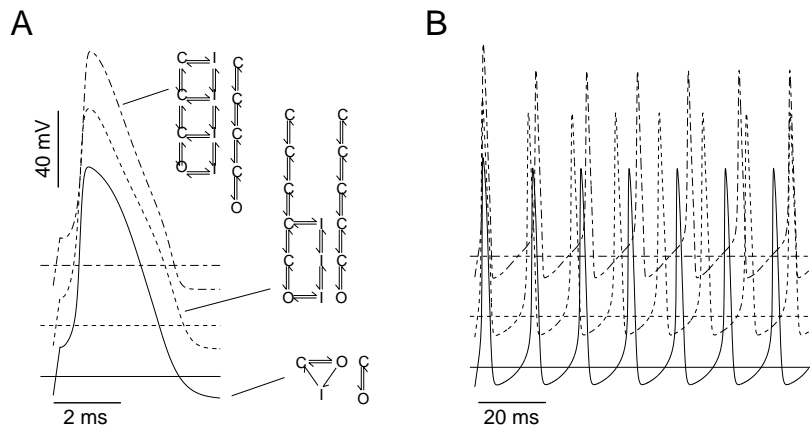


Fig. 3

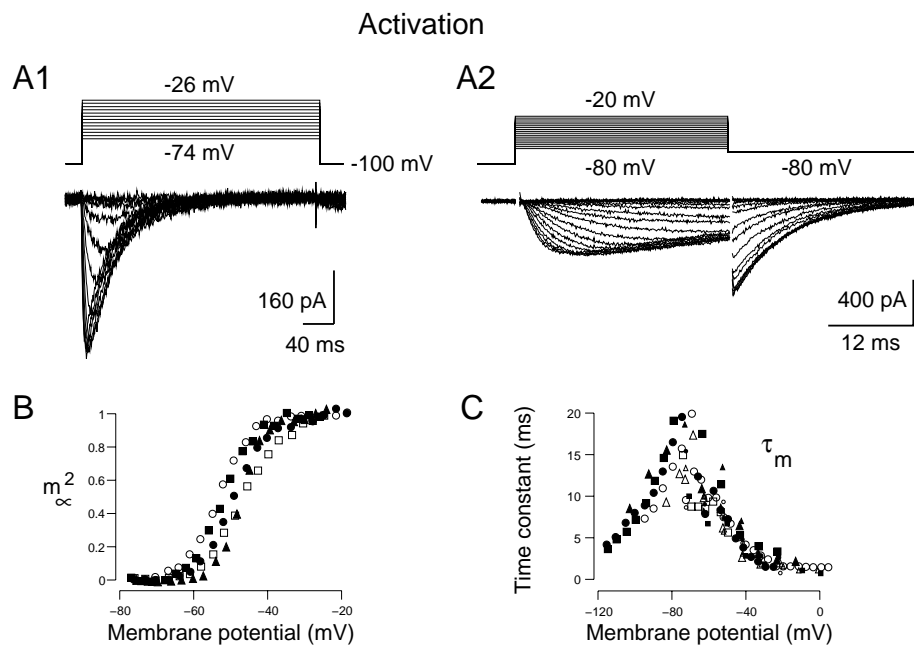


Fig. 4

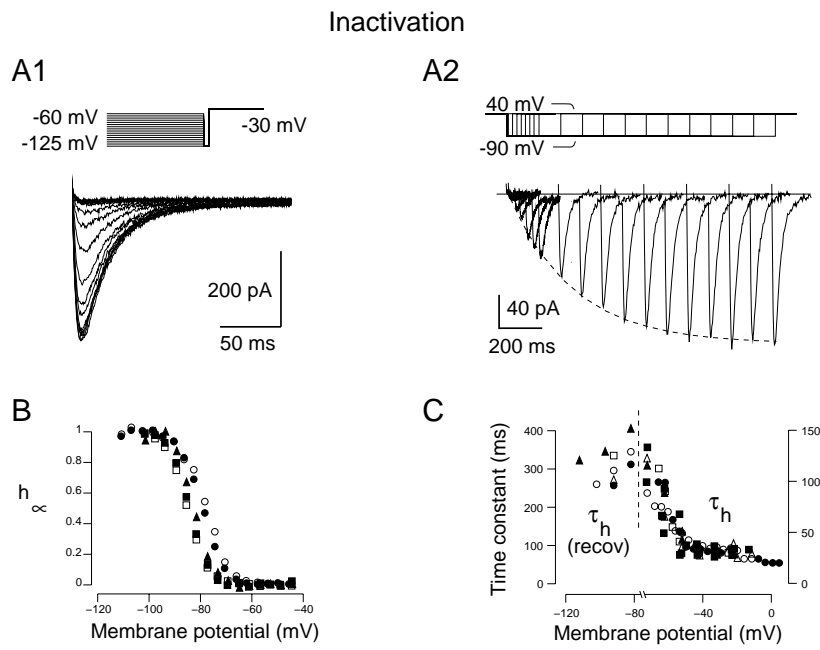


Fig. 5

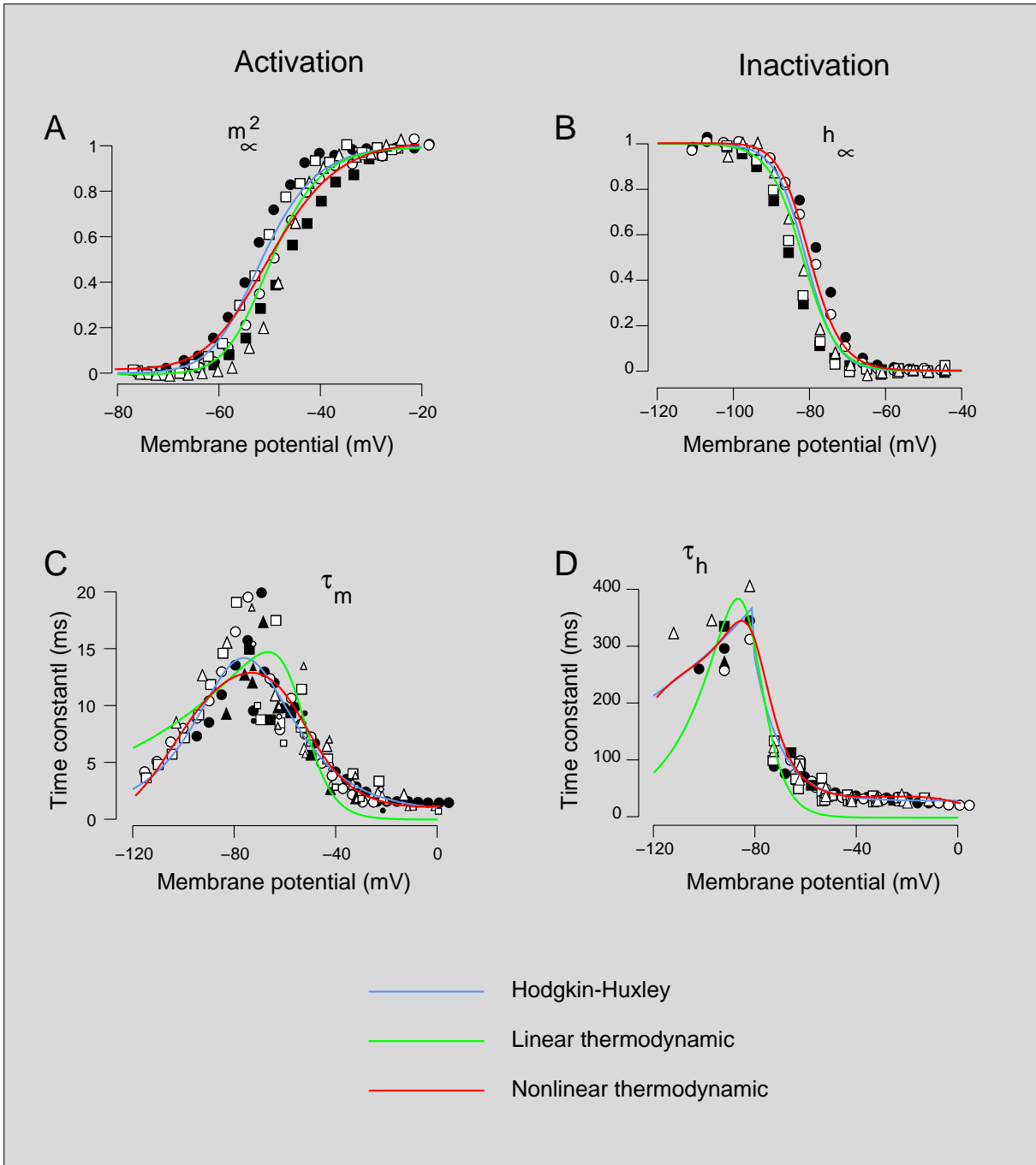


Fig. 6

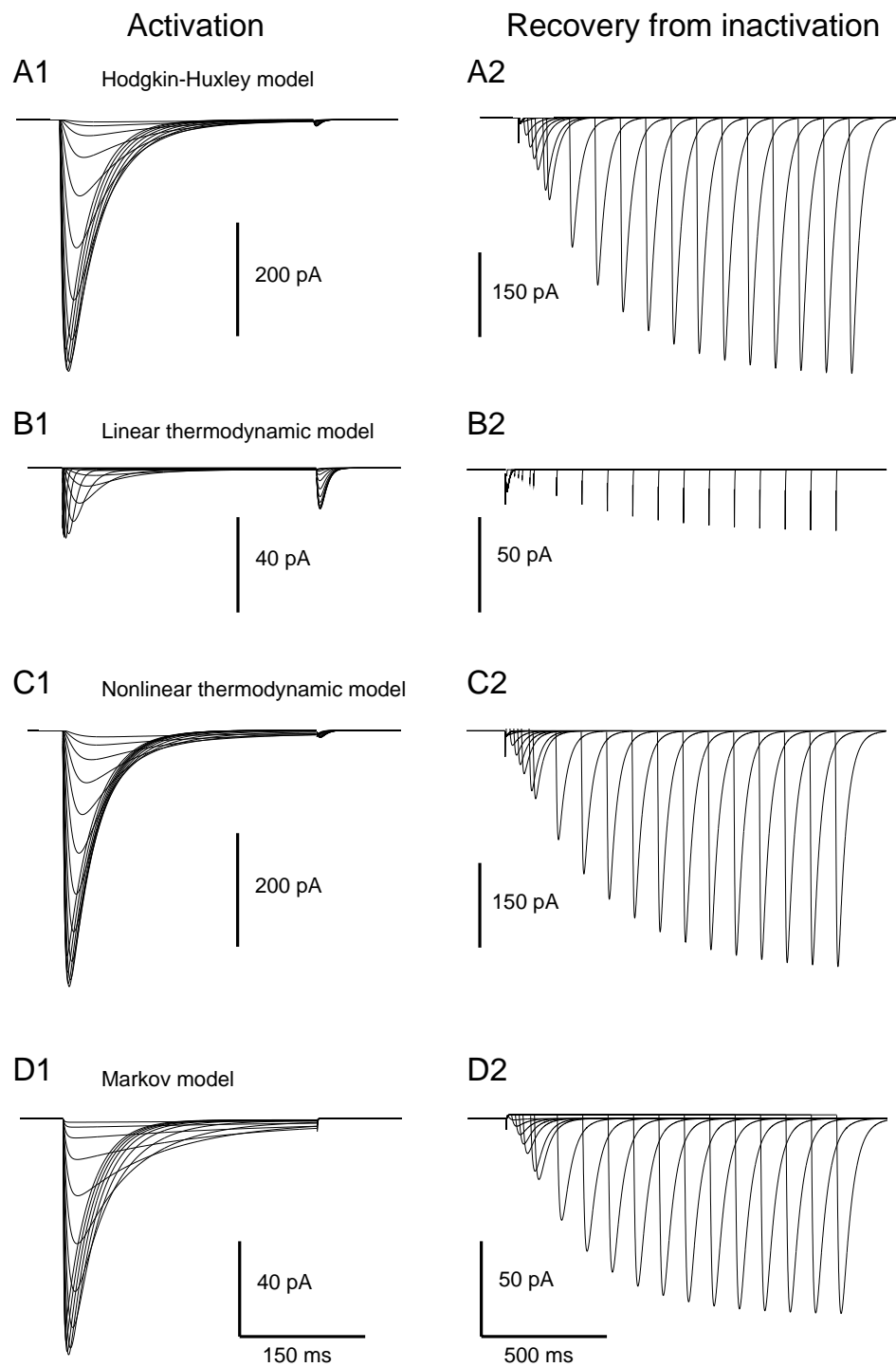


Fig. 7

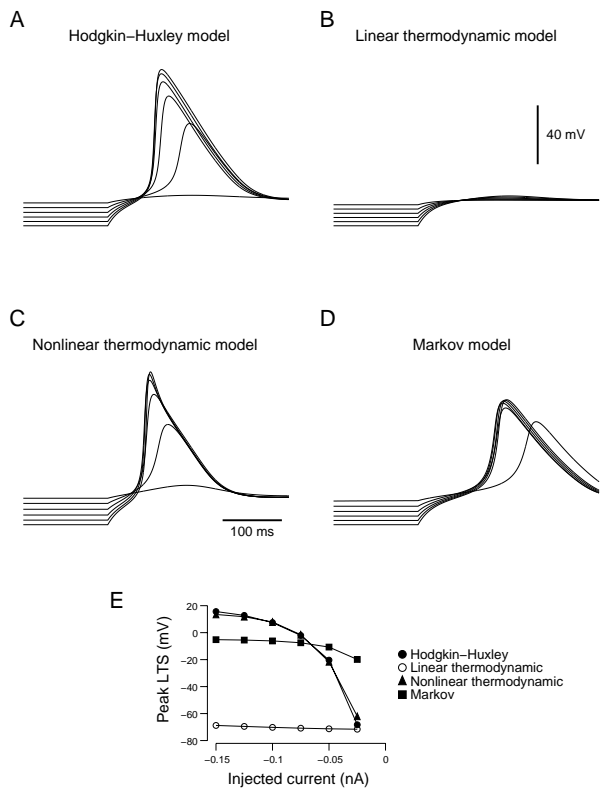


Fig. 8